A Sound Projector for Acoustic Tomography and Global Ocean Monitoring

Andrey K. Morozov and Douglas C. Webb

Invited Paper

***Abstract*—Long-range underwater acoustic systems, such as those used in ocean acoustic tomography, require low-frequency signals covering a broad frequency band. To meet this requirement, a novel design based on of a tunable narrow-band high-efficiency sound projector has been exploited. The projector transmits a frequency sweep signal by mechanically tuning a resonator tube (or organ pipe) to match the frequency and phase of a reference signal. The resonator tube projector consists of a symmetrical pressure-balanced Tonpilz driver placed between two coaxially mounted tubes. The Tonpilz acoustical driver is composed of two pistons separated by preloaded ceramic stacks. The resonant tube is a simple. efficient, narrow-band, medium-output projector that operates at any ocean depth. Both projector tubes have slots (or vents), which are progressively covered or uncovered by sliding coaxial tubular sleeves. The frequency varies with the sleeves position. A computer-controlled electromechanical actuator moves the cylindrical sleeves along the tubes, keeping the projector in resonance at the instantaneous frequency of a swept frequency signal. The actuator smoothly tunes the frequency of the resonator tube in the bandwidth of 200 to 300 Hz during a 135-s transmission. A computer synthesizes the linear frequency-modulated signal; compares the phase between transmitted and reference signals; and, using a phase-lock loop (PLL) system, keeps the resonator tube frequency in resonance with the driver frequency. The estimated PLL precision is better than 3° phase error. The system was analyzed by means of finite element analysis and electrical equivalent circuit simulation. The projector prototype was first tested at the Woods Hole Oceanographic Institution (WHOI) dock in Woods Hole, MA and later in the Pacific Ocean during a voyage of the R/V "Point Sur," November 2001.**

***Index Terms*—Acoustic tomography, ocean acoustics, sound projectors, transducers.**

I. Introduction

DEEPWATER low-frequency broad-band sound projectors are used in sonar systems, ocean acoustic tomography, and deep-penetration seismic profiling. These applications require a controllable high-power source of sound covering a wide range of frequencies [1]–[5]. Some of these applications operate autonomously at great depths for a long time period and need a highly efficient sound source. High-power low-frequency sound can be transmitted by different means (pneumatic, electric spark, electromagnetic devices, etc. [5]). Piezoelectric ceramic tubes and rings are often applied as deepwater sound projectors, because their characteristics are essentially independent of depth [6]–[8]. Long resonator tubes, or organ pipes, can only radiate low-frequency sound with high efficiency over a short range of resonant frequencies [7], [8]. Many of the above-mentioned applications do not require a simultaneous transmission of a broad-band acoustic-energy spectrum. Different frequencies transmitted in sequence, or swept signals, are appropriate when the investigated medium does not change appreciably over the duration of the transmission [9]. A mechanically tunable resonator tube projector enables the radiation of swept frequency signals with high efficiency, high power, and unlimited operating depth. A computer-controlled electrical actuator keeps the projector in resonance with the swept frequency signal. The same projector can be used for the radiation of different narrow-band or continuous-waves (CW) signals in a wide range of frequencies. This projector combines the efficiency and simplicity of resonant tube projectors with the possibility of using wide frequency ranges. The theory of the tunable resonant tube projector, numerical simulation of its parameters, and the results of the experimental testing of the prototype design are presented in this paper.

II. Frequency-Adjustable Resonator Tube System

The resonant frequency of an organ pipe can be controlled by changing its basic resonator parameters. The controlling parameters include the tube length and wall stiffness, the acoustic properties of the liquid environment, and the cross-sectional area and position of orifices in the tube wall. Methods have been explored that can change the frequency smoothly over a large frequency range without a loss of acoustical energy and with negligible changes to the resonator geometry. The tunable device must move smoothly and accurately and the mechanism must be stiff enough to resist forces due to any unbalance in the acoustic pressure. The losses of rubbing and sliding parts decrease the projector efficiency and must be avoided.

A high-power highly resonant all-depth design was systematically developed by altering the way that the resonant energy is stored, so that a wide system bandwidth can be occupied sequentially. The projector includes a symmetrical pressure-balanced Tonpilz driver with two pistons, separated by preloaded ceramic stacks positioned between two coaxially mounted resonator tubes creating a highly efficient narrow-band projector

Manuscript received August 28, 2002; revised February 14, 2003. This work was supported by Office of Naval Research (ONR) under Small Business Innovation Research (SBIR) Program Topic OSD97-009.

The authors are with Webb Research Corporation, 82 Technology Park Drive, East Falmouth, MA 02536 USA (e-mail: dwebb@webbresearch.com).

Digital Object Identifier 10.1109/JOE.2003.811888

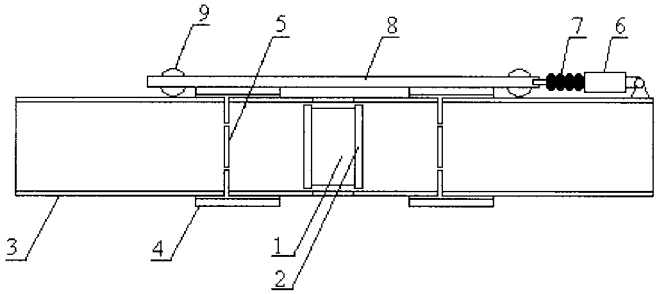

Fig. 1. Resonator tube tunable projector (one wheel, pair 9 of three is shown). 1, a symmetrical Tonpilz transducer; driver with two pistons, 2, separated by preloaded ceramic stacks; 3, resonator tube; 4, coaxial sleeves; 5, orifices in a form of slots (see also Fig. 7); 6, electrical linear actuator; moving metal bar, 8, with wheels, 9, along the resonant pipe, 3; bar, 6, is fastened with the sleeves, 4; 7, rubber oil-filled bellows.

that can operate at any depth. This design is shown in Fig. 1. The initial design is a simple low-cost system consisting largely of aluminum and other environmentally benign materials. The projector was thoroughly tested at the Seneca Lake facility in New York state. A high performance was realized at a frequency of 230 Hz; specifically, we measured a sound pressure level (SPL) +197 dB, an efficiency of 67%, a directivity gain of 3.1 dB, and no sensitivity to pressure. The directivity diagram of this projector is shown in Fig. 2.

To change the resonant frequency of the projector, the resonator tubes were fitted with slots (or vents) at a distance of one-third the resonator tube length measured from the acoustical driver. According to the USA patent [10], the resonance frequency of such vented resonant tube projectors depends on slot sizes and positions. The present projector configuration was decided upon after testing a number of different experimental resonator tubes with varied slot shapes and sizes at the WHOI dock. The final projector design is a configuration of two slotted resonator tubes driven by a coaxially mounted symmetrical Tonpilz transducer. Two stiff coaxial tubular sleeves of larger diameter move axially along the resonator tubes, changing the exposure of the slots (Fig. 7). The inertia of the water layer in the gap between the two coaxial tubes depends on the position of the sleeves relative to the tube slots. The position of the sleeves causes a change in the equivalent acoustic impedance of the slots, thus changing the resonant frequency. As a result, the resonant frequency varies with the position of the sleeves relative to the slots. A computer-controlled actuator moves the sleeves and keeps the projector in resonance with a swept frequency signal. The tunable projector's acoustical physics and parameters can be simulated and predicted by a simple numerical model.

III. Numerical Model of a Tunable Resonator Tube

A theoretical description and analyses of a tunable resonator tube can be accomplished with finite element (FE) analysis, in a two–dimensional (2-D) cylindrically symmetric approach. Fig. 3 shows an example of an FE analysis of a sound pressure level inside the resonant pipe with orifices and moving sleeves. A tunable resonant tube model was bounded by a sphere with an outgoing Sommerfeld radiation boundary condition on this outer sphere to reduce reflections. The FE analysis allows one to calculate the sound pressure level inside the resonator tube, taking into account small details of design and fine effects such as absorption due to water viscosity. The sound pressure calculation at different frequencies shows that the resonant frequency depends upon the position of the sliding sleeve and explains the frequency tuneability. Also, a simplified equivalent circuit model was successfully applied during the experimental design of the prototype projector. This approach has a clear physical basis and will be used to demonstrate the operational capability of the research system.

A simplified model of the resonator tube-tunable projector is based on the similarity of mechanical differential equations and equations for ordinary electrical elements such as capacitors, inductors, resistors, and transformers [11]. The model is simpler than FE analysis and does not need special software or powerful computers to facilitate the prediction of precise projector parameters. This model was continuously compared with the experimental data from the actual projector test. The comparison showed that it truly reflects the organ–pipe sound physics. In this model, we did not take into account the inertia of the aluminum pipe walls, the losses in the walls, the deformation of the Tonpilz transducer shell and the radiation from the orifice, and other small details of the actual projector performance.

Let us assume that a Tonpilz acoustical driver includes m ceramic stacks in a cylindrical form composed of n piezoelectric ceramic longitudinally polarized cylinders. The entire area of the ceramic stacks is A_c. The length of one ceramic cylinder is t_c and the length of all the stacks is l_c. The piezoelectric ceramic polarization direction (3 by convention) is in the axial direction. The reduced constitutive relations [11] for a piezoelectric ceramic are shown in the simple

$$\begin{aligned} S_3 &= s_{33}^E T_3 + d_{33} E_3 \\ D_3 &= \varepsilon_3^T E_3 + d_{33} T_3 \end{aligned} \tag{1}$$

where S_3 is the 3-strain component, T_3 is the 3-stress component, E_3 is the electric field in the 3 directions, and D_3 is the electric displacement in the 3 directions. The piezoelectric material properties are given by compliance s_{33}^E, piezoelectric strain coefficient d_{33}, electric permittivity ε_3^T, and the density ρ_c. The ceramic stack emits sound pressure with a frequency f into the water through a piston with area A_p, length l_p, and material density ρ_p.

The acoustic Tonpilz driver is placed between a pair of open-ended cylindrical tubes with individual length L, cross-sectional area A, and thickness h. Each section has orifices with the area A_o formed in the walls at a distance L_o from the acoustic driver. The movable coaxial sleeve has a length l_s and radius g, which is larger than the radius of the main tubular section. The projector tubes are free flooded with water (density ρ_o and sound velocity c_o).

The electrical lumped-equivalent circuit for one-half of the symmetric resonator tubes is shown in Fig. 4, where $C_b = nA_c\varepsilon_{33}^T(1-k_{33}^2)/t_c$ is the capacity of the piezoelectric ceramic for a clamped circuit; $C_b = nA_c\varepsilon_{33}^T/t_c$ is the same capacity for an open circuit; $k_{33} = d_{33}/\sqrt{\varepsilon_{33}^E s_{33}^E}$ is the coupling coefficient (a property of the piezoelectric ceramic material); $C_m = l_c s_{33}^E A_p^2/A_c$ is the ceramics stiffness equivalent capacitor; $L_m = L_c + L_p = 4\rho_c A_c l_c/A_p^2\pi^2 + \rho_p l_p/A_p$ is

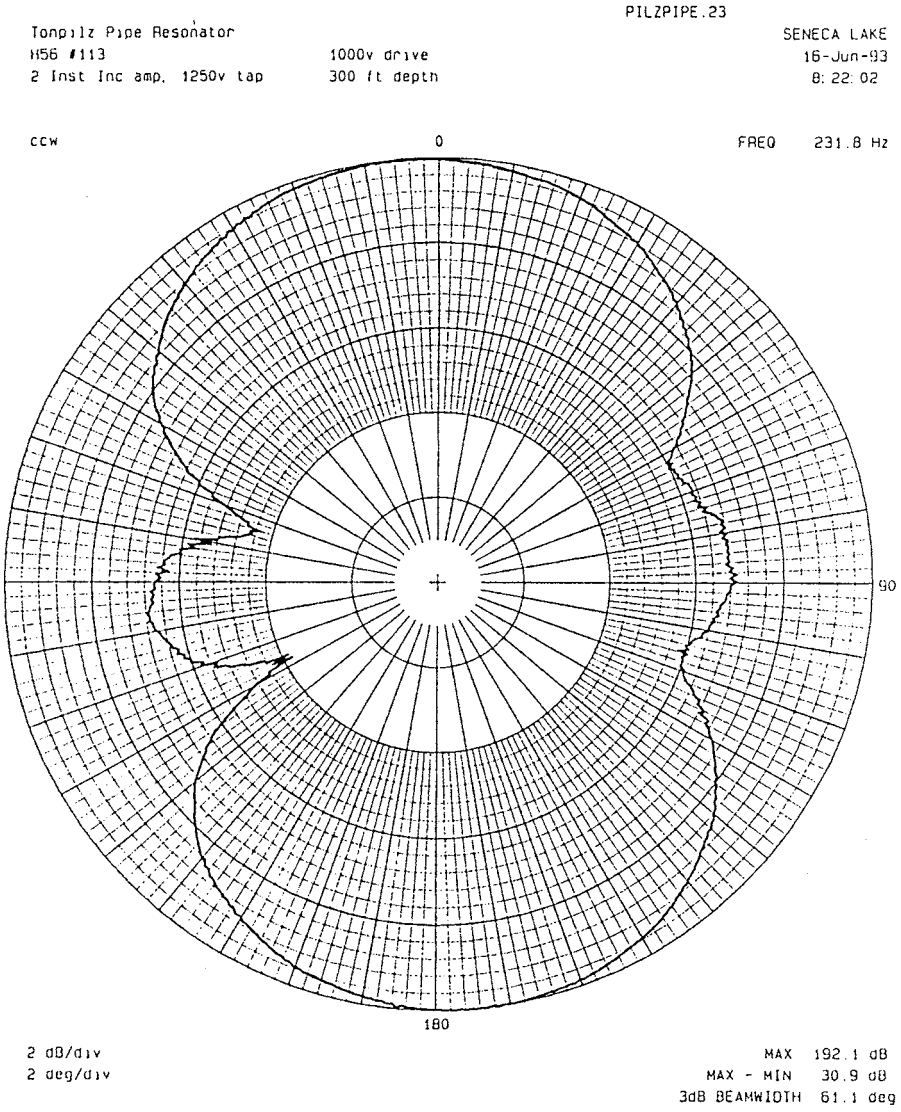

Fig. 2. Index of intensity directivity of a resonator tube projector.

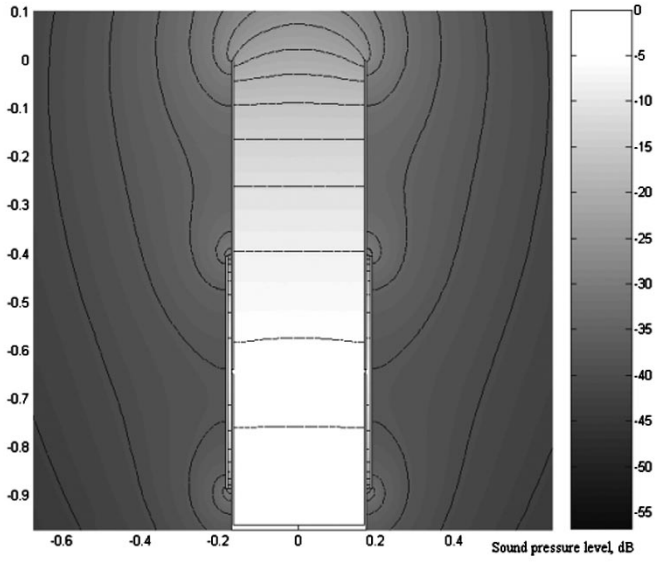

Fig. 3. Finite element modeling of sound pressure (in dB reacoustical transducer level), showing one-half of the symmetrical projector assembly.

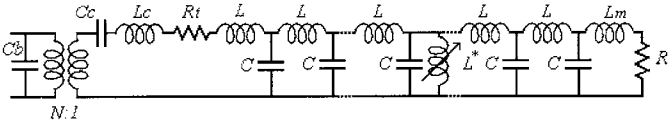

Fig. 4. Resonator tube projector equivalent circuit.

the lumped equivalent inductance of the combined ceramics and piston inertia; $R_t = (1 - A_c/A_p)^2 \pi \rho_o f^2 / c_o$ is the radiation resistance from the Tonpilz center; $N = d_{33} A_c / (A_p s_{33}^E t_c)$ is the transformation coefficient; A_p is the piston area; $L = \rho_o d / A$ is the inertia of the water mass in the tubular section with the length d; $C = C_{\text{water}} + C_{\text{wall}} = A\beta d + 2ARd/(Eh)$ is the combined capacitance of the wall stiffness and water compressibility; $d = L/k$ is the length of one section where k is the number of sections in the numerical model, L is the length of the tube, and L^* is the variable inductance equivalent for the water inertia in the gap between the resonator tube and the movable sleeve; $L_m = 0.25 \rho_o \sqrt{\pi / A}$ is the inductance of the added mass of the open resonator tube end; and $R = \pi \rho_o f^2 / c_o$ is the radiation resistance [11].

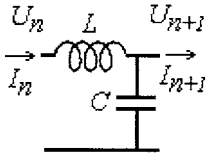

Fig. 5. The electric circuit model of an elementary segment of a resonator tube.

The key element of the projector design is the variable inductance L^*. The inductance is derived from the position of the movable sleeve relative to the position of the slot in the resonator tube. When the slot is completely uncovered this inductance can be calculated from (2) for the added mass m of the open orifice, which is

$$m = 0.5\rho\sqrt{\pi}A_o^{3/2}. \tag{2}$$

When the moving sleeves close the slots, the inertia of the water in the gap between the resonator tube and the sleeve is increased. The resulting dependence of the variable inductance L^* on the displacement for a circular orifice can be approximately represented by the following (3), where x is the displacement of the movable sleeve from the center position.

$$L^* = \frac{\rho_o}{2}\sqrt{\frac{\pi}{A_o}} + \frac{\rho_o\,(0.5l_s - x)\,(0.5l_s + x)}{2\pi r g l_s}. \tag{3}$$

A short segment (Fig. 5) of a resonator tube with length dX is simulated by an LC resonant circuit, which can be described by a simple matrix

$$\boldsymbol{V}_{n+1} = \boldsymbol{A}V_n \tag{4}$$

where

$$\boldsymbol{V}_n = \begin{bmatrix} U_n \\ I_n \end{bmatrix},\ \boldsymbol{V}_{n+1} = \begin{bmatrix} U_{n+1} \\ I_{n+1} \end{bmatrix}$$
$$\boldsymbol{A} = \begin{bmatrix} 1 & -i\omega L \\ -i\omega C & 1-\omega^2 LC \end{bmatrix}.$$

The admittance of the resonator tube can be calculated from the continued fraction

$$y = i\omega C_b + \frac{N^2}{i\omega L_c + \frac{1}{i\omega C_c} + R_t + z} \tag{5}$$

where

$$z = i\omega L + \cfrac{1}{i\omega C + \cfrac{1}{\cdots \cfrac{1}{i\omega L + \cfrac{1}{i\omega C + \cfrac{1}{i\omega L^* + \cfrac{1}{\cdots \cfrac{1}{i\omega C + \cfrac{1}{i\omega L_m + R}}}}}}}}.$$

The radiated volume velocity and pressure sound level p_{spl} can be calculated by the following matrix:

$$\begin{aligned} U_1 &= U_0 N;\ I_1 = \frac{U_0 N}{z}; \\ \mathbf{V}_1 &= \begin{bmatrix} U_1 \\ I_1 \end{bmatrix};\ \mathbf{V}_k = \begin{bmatrix} U_k \\ I_k \end{bmatrix}; \\ \mathbf{V}_k &= \mathbf{A}^{k-k_o}\begin{bmatrix} 1 & 0 \\ \frac{-1}{i\omega L^*} & 1 \end{bmatrix}\mathbf{A}^{k_o}\mathbf{V}_1; \\ P_{\mathrm{spl}} &= 20\mathrm{Log}_{10}\left(\rho_o f\,|I_k|\right). \end{aligned} \tag{6}$$

TABLE I
PIEZOELECTRIC TONPIL-DRIVER AND RESONATOR-TUBE PARAMETERS

Piezoelectric Tonpilz driver parameters		Resonator tube parameters	
t_c, m	0.0127	L, m	1.397
l_c, m	0.0762	A, m^2	0.08899
A_c, m^2	0.081	h, m	0.0095
s_{33}^E, m^2/n	$18.5\cdot10^{-12}$	L_0, m	0.4572
ε_{33}^T, m^2/n	$11510.2\cdot10^{-12}$	A_0, m^2	0.0768
d_{33}, k/n	$253\cdot10^{-12}$	g, m	0.002
ρ_c, kg/m^3	7500	l_s, m	0.02
l_p, m	0.06985	ρ_0, kg/m^3	1005
ρ_p, kg/m^3	2700	c_0, m/s	1490
A_c, m^2	0.061311		
n	6		
m	4		

The simulation example of a tunable resonator tube was accomplished with the following parameters, shown in Table I.

The input projector voltage was $U_0 = 1500$ V, $n = 6$, $m = 4$. The dependence of the sound pressure level of 1 μPa at the distance of 1 m from the position of the movable sleeve is shown in Fig. 6. The displacement of the sleeve was changed in 2-mm steps. The resonant frequency depends on a sleeve position changing fluently and can be tuned to any frequency in the range of 200 to 300 Hz. The model gives a good qualitative assessment of the bandwidth and other resonator tube projector properties. The exact dependence of the resonant frequency on the sleeve displacement x is strongly determined by the form of the slots and cannot be precisely described by this simple model. The final geometry of the orifice was determined during experimental testing of the projector prototype.

IV. EXPERIMENTAL TESTING OF THE TUNABLE RESONATOR TUBE

A series of experiments was conducted to search for the optimum slot design and to test the actual parameters of the tunable resonator. The resonator tube-projector prototype was submerged in water to a depth of approximately 8 m. An SR785 signal analyzer was used to measure transducer admittance at low power and to determine the performance of the projector. All other projector parameters were as described in the theoretical model.

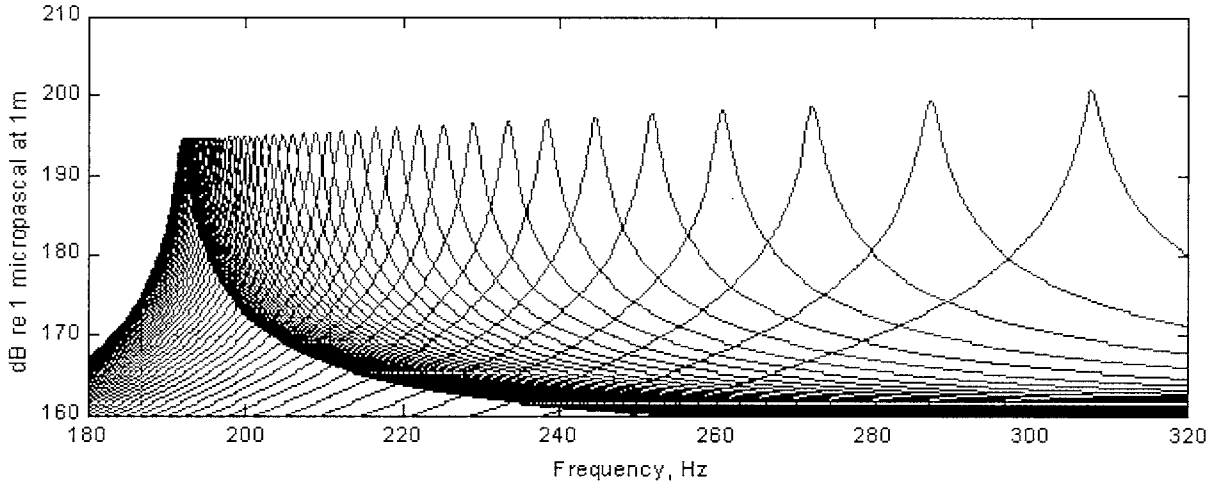

Fig. 6. The sound pressure level of a tunable resonator tube for different positions of a movable sleeve; the difference between any two displacements is 2 mm.

The position of the movable sleeve displaced by an electric linear actuator was measured with a potentiometer. The electric actuator, potentiometer, and Tonpilz transducer were cable connected to test measuring equipment. The experiment was performed using different tunable resonator tube parameters. The length of the movable sleeve was varied over the range of 20 to 26 cm. The gap between the resonator tube and sleeve was varied over the range of 1 to 12 mm. The sleeve thickness was changed in the range of 12.6 to 25.4 mm. Different shapes of resonator tube slots were also tested. The system was tested in a frequency range of 185 to 350 Hz. In comparing the data obtained with the results of numerical calculations, it was shown that a simple model, in the form of an electrical circuit, predicts results and explains the observed properties of resonators adequately. For a precise description of the acoustic properties of the resonator in all frequency ranges, it is necessary to have a more complicated model of the opening slot impedance. The opening slot profile was, thus, modeled by means of FE analysis. As a result of the experimental research on the projector with a controlled resonator, the optimal parameters of the movable sleeve were determined. These parameters were used in the calculations example shown above. These parameters allow frequency changes in the range of 200 to 300 Hz, free from other resonant frequencies.

The experimental research showed that circumferential slot orifices with rounded edges are more effective than circular ones (Fig. 7). The long slot design needs a smaller area for the same effect as a round orifice. The dependence of the resonant frequency on the movable sleeve position with long slots is stepless and smooth. The smooth shape of the slots is important for decreasing viscosity losses and turbulent effects during high power radiation. The series of frequency-dependent admittance curves for the final resonator tube projector design, taken directly from the SR785, are shown in Fig. 8.

The resonant frequency dependence on the movable sleeve position for two different design variants is shown in Fig. 9. These designs differ in the width of the gap between the resonator tubes and the sleeves: the marker $\circ$ corresponds to a gap $g = 0.002$ m, while the marker Δ corresponds to a gap $g = 0.0015$ m. Both systems have approximately the same bandwidth and both can be used for linear frequency sweeping across the band. A system with a small gap ($g = 0.0015$ m) closes the slot more tightly and, as a result, the whole bandwidth is shifted at low frequencies. The system with the small gap ($g = 0.0015$ m) also does not close the orifice completely, but displays very smooth dependence of the resonant frequency on the position of the movable sleeve. Such a smooth dependence is preferable for the PLL feedback.

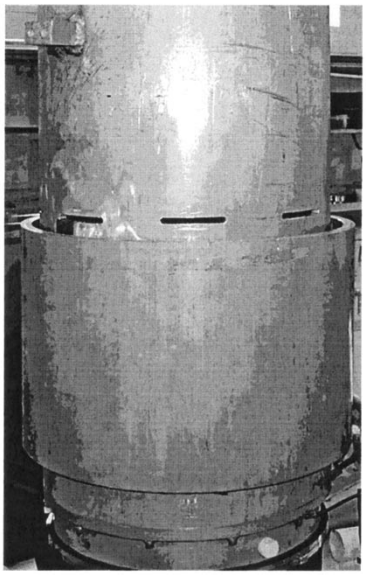

Fig. 7. The resonant pipe with the open orifice in a form of slots.

The Q factor of the resonator ($Q = f/(2\Delta f)$) is shown in Fig. 10. The tunable projector has approximately the same efficiency as the basic resonator tube without slots and a movable sleeve. A nearly constant frequency bandwidth of the resonance curve ($2\Delta f \approx 2$ Hz) for different resonant frequencies is an advanced and attractive property of the design.

As a whole, the experiments show that the resonator tube projector with additional slots and movable sleeves maintains the high efficiency of the original resonator tube and can be

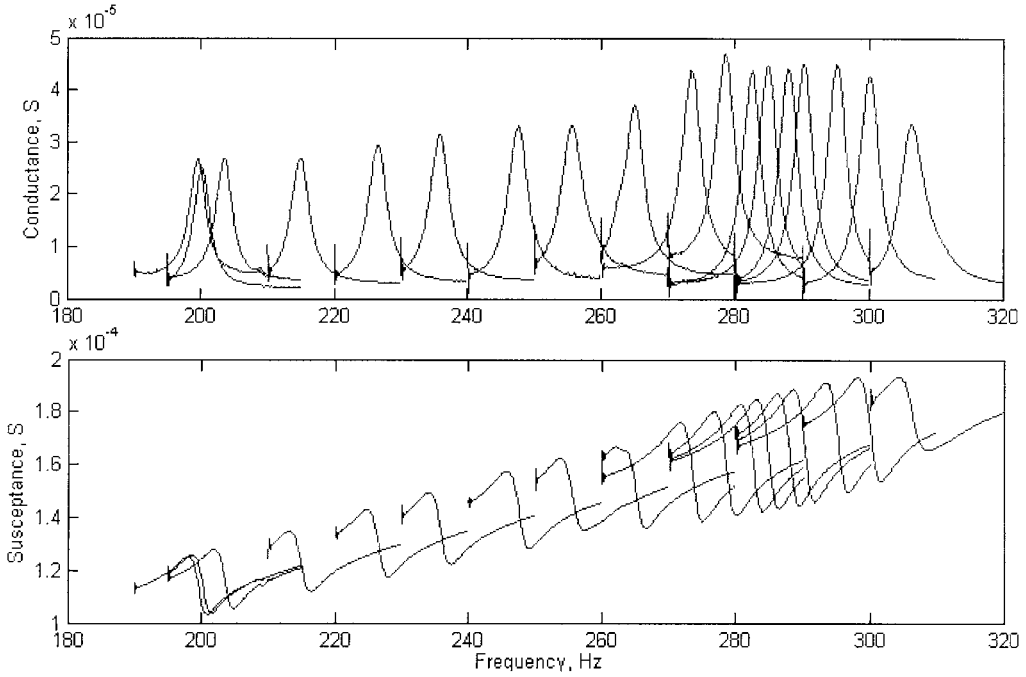

Fig. 8. Experimentally measured admittance of the projector for different positions of the movable sleeve.

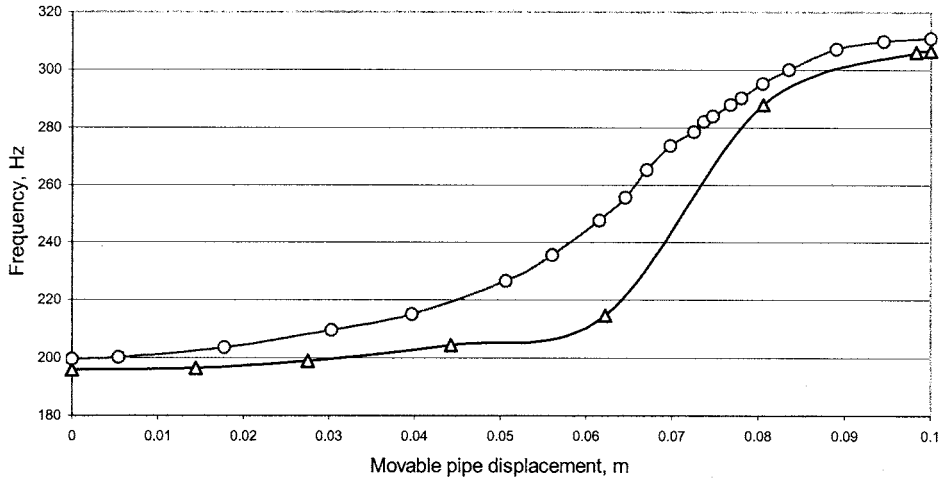

Fig. 9. Resonant frequency dependence on the shift of the movable ° $g = 0.002$, $\Delta g = 0.0015$ m.

smoothly tuned in a frequency bandwidth of more than 200 to 300 Hz. Such a projector can be used for the radiation of a CW waveform with different frequencies or for any kind of a sweep along the frequency bandwidth.

The projector must be tuned to resonance in real time by an electromechanical actuator. For example, it can be accomplished by using a microprocessor, which synthesizes the signal, reads the position of the movable sleeve with a positioning potentiometer, and moves the sleeve in accordance with a position-frequency table. Fig. 9 helps to answer the question of how precise the mechanical actuator must be. From the black curve, we can estimate that the resonant frequency changes 4 Hz when the sleeve is moved 1 mm. The precision must be at least 0.1 mm. Such precision can be realized, but it is not a simple design. Taking into account that the resonant frequency of a free-flooded resonator tube depends on temperature, salinity, and corrosion of the surface, it becomes clear that the system must be self-regulated. The negative feedback from the output of the electromechanical actuator can correct all possible changes in the resonant frequency and keep it in accordance with the instantaneous frequency of the transmitted signal.

V. Resonance-Frequency PLL Regulator

One specific property of the resonator tube projector is that it uses seawater for acoustic energy storage. It makes the projector lightweight, but it also makes the resonant frequency dependent on environmental parameters. The projector-resonant frequency depends on seawater temperature and on the tube surface condition. The tube can be covered in the first minutes after submer-

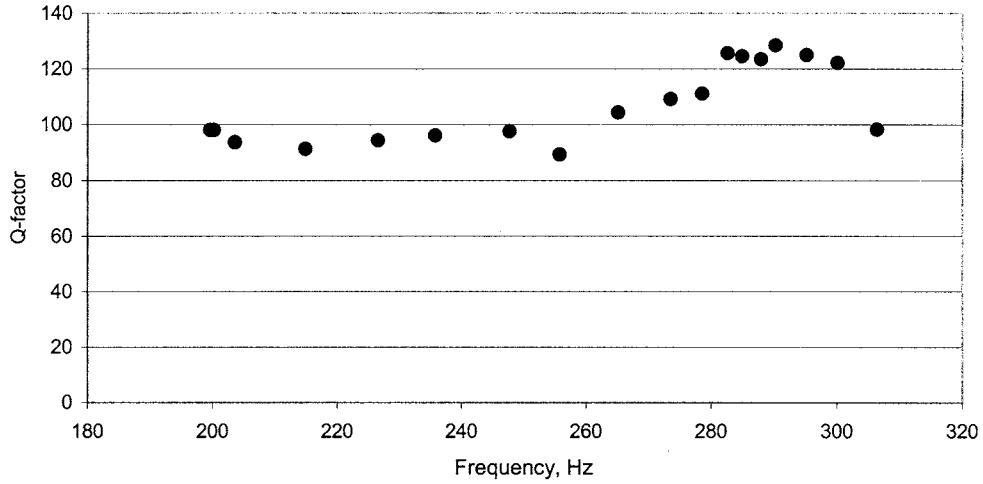

Fig. 10. Q factor of a tunable projector in the optimal-frequency band.

gence by microbubbles or it can corrode during exposure in the sea. Automatic resonant frequency tuning of the projector can stabilize the system against variations of water properties and tube surface conditions.

Two different approaches are possible for the creation of an acoustic projector on the basis of a tunable resonator.

- The resonator and its drive circuit are self-resonant and this circuit is tuned by moving the sleeves to track the reference signal.
- One can drive the resonator with the reference signal and move the sleeve to maintain the resonator at peak output.

A comparison of both approaches using a computer numerical model shows that the second method has less dynamic errors and, thus, the second method is preferred. Accordingly, the signal was synthesized in a microcomputer in digital form. After the power amplifier, the signal goes to the tunable resonator tube projector, controlled by a PLL [12]. A signal from the output of the power amplifier and the matching filter was used as a reference signal. It is presumed that the compensation chains of the projector's capacitance C_b do not have significant phase error.

This scheme allows usage of a nearly perfect, direct, digitally synthesized signal from the computer system on the input of the transducer. The PLL automatically follows the instantaneous frequency of the emitted signal, thereby tuning the resonant frequency of the projector. Thus, the instantaneous frequency of the radiated signal is always in the center of the projector's "transparent window," in which the transformation of electric energy to acoustic energy is at the highest efficiency.

Phase discrimination is a very important consideration in the design of the PLL resonant-frequency control for the resonator tube projector [12]. The electric current through the piezoelectric transducer consists of two components: 1) current flowing through the capacitance C_b and 2) current due to the electrical charges caused by the displacement in the piezoelectric ceramics. The phase difference between the voltage on the transducer input and charge displacement current changes the sign when the signal frequency is equal to the resonator tube resonant frequency. This phase can be a good indicator of the resonance. The charge displacement current can be extracted from the transducer line current with the help of a ceramics capacitor current compensation circuit.

Such a compensation circuit was worked out and tested. The main advantage of the frequency PLL, with the transducer capacitor current compensation circuit, is its simplicity. The computer captures the zero-level crossing time for voltage and displacement current and calculates the time interval between these two moments. This value is filtered and controls the electrical actuator moving the sleeve. The motor runs until the voltage and the compensated current are in phase, thereby tuning the resonator tube to the resonant frequency. The dependence of the compensation circuit on temperature, pressure, and length of the cable and the necessity for precise tuning are the disadvantages of this method. As shown in Fig. 8, the capacitor C_b current is several times larger than the displacement current. The line current becomes much less after the subtraction of the capacitance current component. The result of the subtraction depends heavily on any variations in the compensation circuit. After testing the compensation circuit, it was decided to not use it and to choose another kind of PLL.

In the second scheme, the voltage phase at the piezoelectric transducer entry was compared with the voltage from a small hydrophone placed in one of the resonator tubes in the vicinity of the Tonpilz driver. In Fig. 11, one can see the ratio $H = U_h/U_0 = H_r + iH_i$, where U_0 is the voltage on the piezoelectric transducer, U_h is the voltage from the hydrophone, H_r is the real part of ratio (black curve), and H_i is the imaginary part (gray curve).

The electrical voltage from the hydrophone is in quadrature with the transducer input voltage at the resonant frequency. This means that the hydrophone voltage is the ideal signal for an automatic frequency-control system based on a PLL. The signal from the hydrophone and the input transducer voltage can be compared in a phase discriminator whose output voltage will be proportional to their phase difference. After filtering, this voltage drives an electric motor that displaces the movable sleeve toward the resonant position. The above-mentioned filter

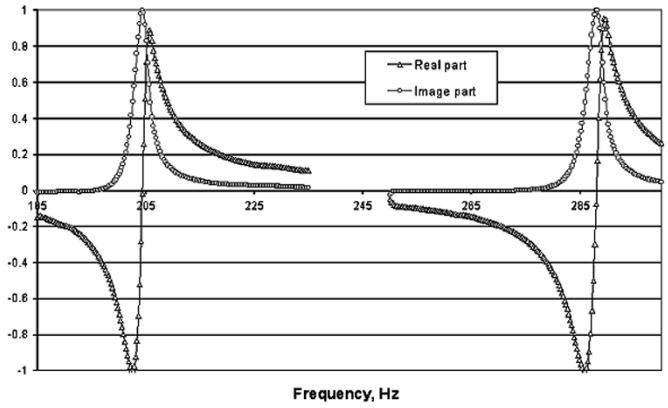

Fig. 11. The input-to-hydrophone voltage ratio for different positions of movable sleeve: left, displacement 4 cm; right, displacement 7 cm.

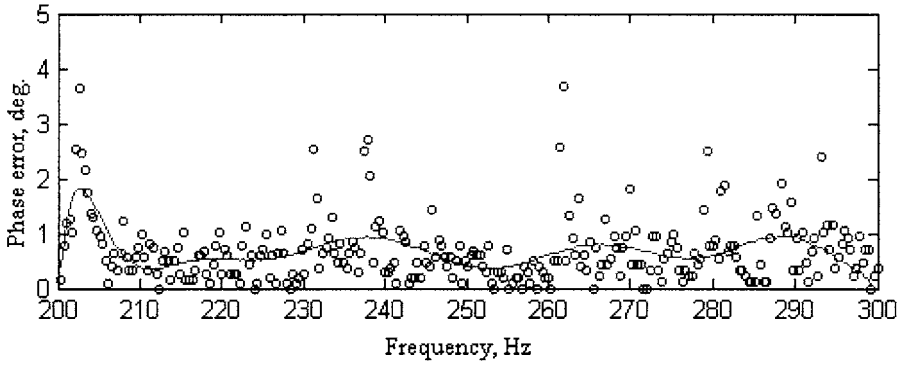

Fig. 12. Amplitude of PLL dynamical phase error, measured during ocean testing.

determines the dynamic properties of the PLL. The filter can be realized in accordance with the

$$x_n = x_{n-1} + 0.005\,(\varphi_{n-1} - x_{n-1})$$
$$y_n = 0.25x_n + \varphi_n + 0.75\langle y_n\rangle \qquad (7)$$

where φ_n is a sample of the signal from the discriminator at a time moment t_n, x_n is the signal after discrete filtering, y_n is the motor-control signal, and $\langle y_n\rangle$ is the motor control signal averaged for a few periods of previous sweeping. The digital PLL operates with a discrete interval equal to the sweeping signal period $\Delta t = 1/f$. The algorithm was implemented using a program for a microprocessor system and was tested in a digital model for different sweeping signals.

The result of testing the PLL system *in situ* is shown in Fig. 12. The PLL errors shown by dots were taken in 0.5 s intervals. The solid curve is the least squares fitting. The small phase error of the PLL resonance-control system allows for the achievement of a very high coherence of the transmitted signal and, as a result, a very high correlation with the reference signal.

The signal high coherence is confirmed by the correlation between received and reference signals at different delays. The comparison of experimental and theoretical correlation functions was done during WHOI dock testing. The result is shown in Fig. 13. The experimental curve complies well with the experimental data. The difference in side lobes is explained by the reflections of sound from the sea surface and ocean bottom in shallow water conditions.

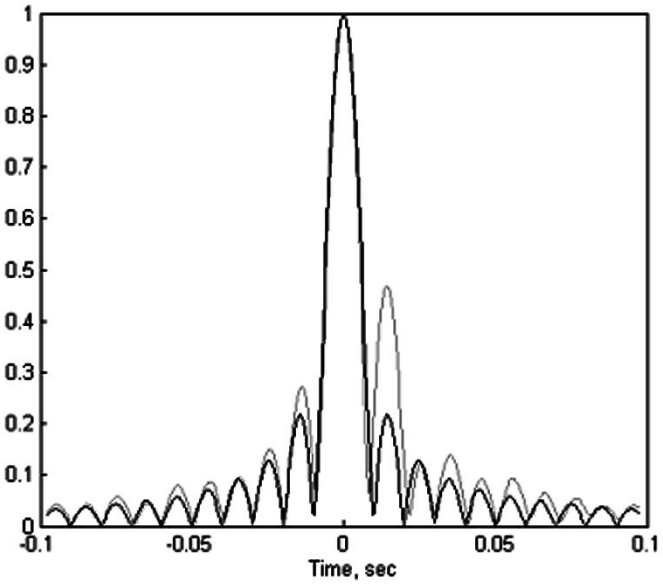

Fig. 13. Correlation function, measured at the WHOI dock at the depth of 8 meters.

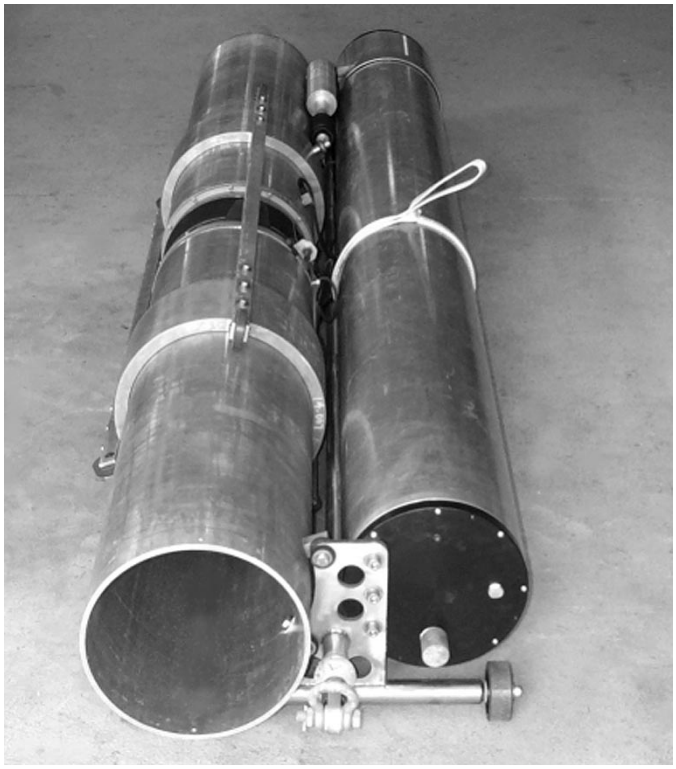

Fig. 14. Sound source system.

VI. An Autonomous Long-Term System Design for the Application of a Broad-band Swept Frequency

Based on the previous tests, a complete swept frequency projector system for long-term deployment in the sea was designed and developed. The system was developed to be used as part of an acoustic ocean tomographic system with path lengths of up to 1000 km. The system consists of a swept frequency projector and a rigid housing containing batteries and control electronics.

The resonator tube projector consists of two 138-cm-long free-flooded tubes with an external diameter of 0.3556 m and a wall thickness of 0.009 m (see Fig. 14). The symmetrical Tonpliz transducer is placed between these two tubes. The movable sleeves have inner diameters 1.5 mm larger than the external diameter of the resonator tubes and have a wall thickness of 0.0254 m. The electronics hull is cylinder with the 0.305-m diameter and 3.048-m length from a 6061-T6 aluminum alloy. Both ends are covered with hard anodized end caps. The total weight of the system, with a full battery compliment, is 500 kg in air and 220 kg in water.

Potentially, the projector can be used to effectively radiate signals with continuous phase and constant amplitude for any swept frequency in the range of 200 to 300 Hz. This particular sound-source system uses a tomography broad-band 200- to 300-Hz linear-frequency swept signal and a RAFOS narrow-band frequency swept signal. RAFOS is a system of neutrally buoyant floats that are tracked by long-range acoustic positioning systems. The chirp signal of the RAFOS system is used to measure sound pulse travel time from a moored sound source to a floating buoy. The RAFOS signal is a narrow-band linear frequency, swept from 259.375 to 260.898 Hz for 80 seconds. For tomography, the broad-band linear-frequency swept signal changes its frequency from 200 to 300 Hz during 135 seconds. In both cases, the frequency sweep is generated in a direct digital synthesizer by switching CW signals every 50 ms. The projector can be reprogrammed to transmit a different CW or narrow-band signal with arbitrary frequency in the range of 200 to 300 Hz or virtually any kind of slowly swept signal. This makes it useful for a number of different acoustical measurements and applications.

The projector's maximum SPL is 195 dB re 1 μPa at 1 m. The projector design maintains the high efficiency of the initial resonator tube, approximately 50%, and a directivity index of more then 3 dB in the horizontal direction.

The sound source electronic system contains a Motorola MC68CK338 microcontroller, a direct digital-signal synthesizer, an H-bridge power amplifier with a class "D" pulse-width modulated (PWM) output signal to the electrical actuator, a class "D" PWM power amplifier driving the Tonpilz transducer, a hybrid rubidium/quartz low-power-consumption clock, internal vacuum pressure sensor and external environmental pressure sensor, a battery energy and leakage sensor, a Serial ASCII Instrumentation Loop (SAIL) open collector (OC) internal interface of the internal system BUS, a SAIL current loop (CL) interface for external control, and an RS232 interface for program loading. The MC68CK338 is a highly integrated 32-bit microcontroller combining a high-performance data-manipulation capability with powerful peripheral subsystems. The microcontroller contains 1 MB of flash memory that acts as the read-only memory (ROM) for the operating system, 256 KB of static random-access memory (RAM), and 48 MB of flash memory card. Power management, with protection circuitry, lets the system drop into an extremely low power mode. The program is written in "C" programming language. An internal BUS on the base of the open collector SAIL interface retains compatibility to the previous tomographic system design and for the system extension. The rubidium–quartz hybrid clock has a long-term stability $< 10^{-9}$.

The movable coaxial sleeves are displacing by a linear actuator. The actuator uses a brash electrical motor with a worm-and-roller gearbox. The gearbox is oil filled, pressure balanced, covered by rubber bellows.

The system is powered by an assembly of alkaline "D" cell batteries with an endurance of 3000 transmissions. The pressure hull is built for an operational depth of 2000 m. The operating depth for the projector is unlimited.

The system was used for the first time in the Pacific Ocean in November 2001 during a cruise of the research vessel "Point Sur." The vessel was positioned in the region of the underwater Hoke Seamount (Fig. 15) and the system was submerged to a depth of 35 m. The projector periodically emitted RAFOS signals and linear frequency-modulated signals in the range of 200 to 300 Hz.

The RAFOS chirp signals were used in the experiment to demonstrate the capability of transmitting not only broad-band swept frequency signals, but also any kind of narrow-band signal with a carrier frequency in the range of 200 to 300 Hz. Each RAFOS chirp signal transmission began with a CW signal used to adjust the projector resonant frequency so as to comply

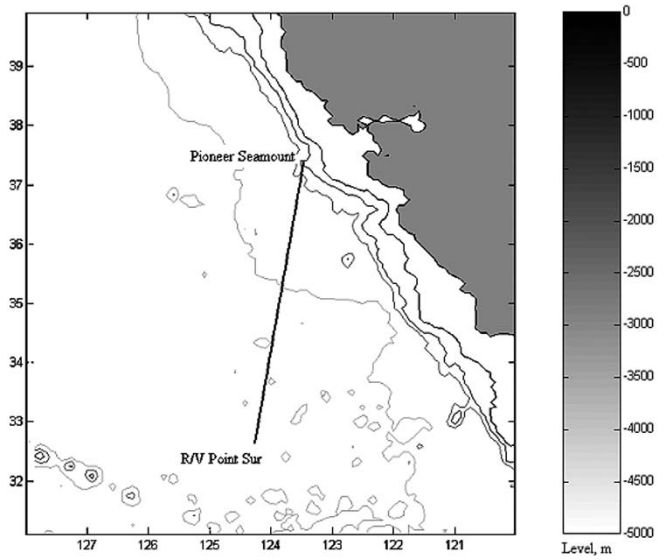

Fig. 15. Site of the initial test experiment.

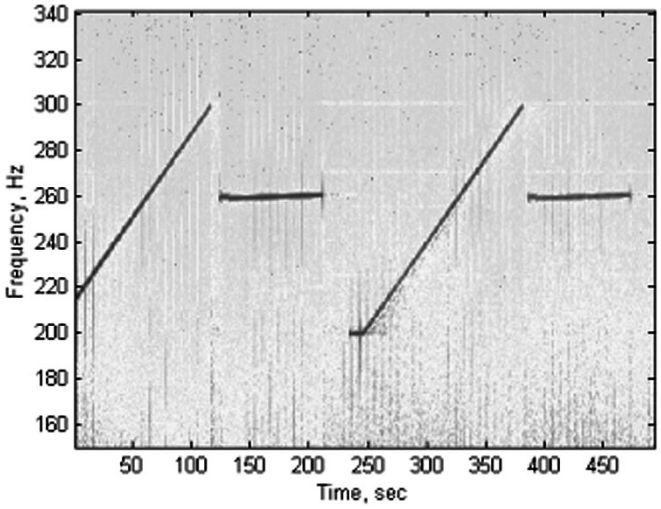

Fig. 16. RAFOS signal and swept frequency signal (200 to 300 Hz), transmitted from R/V "PT SUR" and received by nearby sonobuoy.

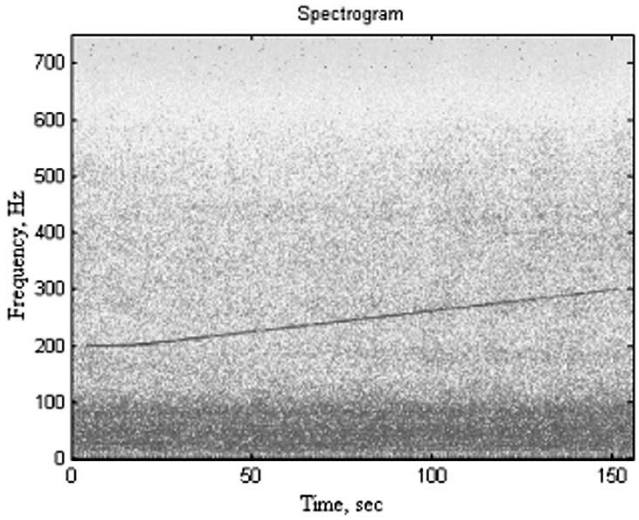

Fig. 17. Spectrogram of the signal received at the Pioneer Seamount receiver.

with the central frequency of the transmitted signal. The PLL self-regulator was switched on during the CW section and the system was tuned exactly to the CW frequency equal to the chirp signal central frequency. At the end of the CW section, the PLL was cut off. The resonant frequency of the projector remained constant and equal to the central frequency of the RAFOS signal during the time of its transmission. The same method can be used to transmit of any kind of narrow-band signal with an arbitrary carrier frequency in the range of 200 to 300 Hz.

The transmission of each broad-band 200- to 300-Hz swept frequency signal begins with a section of CW signal with the carrier frequency 200 Hz. This signal is also used to adjust the resonant frequency of the system before frequency sweeping begins. In this case, the PLL feedback continues to function over the period of the swept signal transmission, keeping the resonant frequency in compliance with the instantaneous signal frequency.

Drifting sonobuoys nearby were used to monitor the signal transmission. The spectrogram of the transmitted signals is shown in Fig. 16. Two kinds of linear frequency-modulated spectrograms from the RAFOS chirp and the broad-band swept frequency are shown in the form of sloping lines.

The signal was also received by a distant acoustical array deployed on a slope of the Pioneer Seamount. The distance between the sound source, located on the research vessel "Point Sur" and the Pioneer Seamount receiving station, was approximately 530 km. The spectrogram of the broad-band swept frequency signal received by one of the hydrophones at the acoustical array is shown in Fig. 17.

The numerical simulation of the acoustic ray trajectories, on the basis of the average data for this time of year, shows that only one ray from the sound source was received without reflection from the surface and the ocean bottom. All other rays were scattered on the slope of the Pioneer Seamount. This ray was used to analyze the broad-band swept signal correlation function in the acoustical source far-field zone.

The optimal estimation of travel time is based on the correlation function of the received signal $x(t)$ and the reference signal $y(t)$. The amplitude of the correlation function of the received and reference signals can be calculated in accordance with

$$c(\tau) = \sqrt{\left(\int_0^{T_c} y_s(t)x(t-\tau)dt\right)^2 + \left(\int_0^{T_c} y_s(t)x(t-\tau)dt\right)^2}. \quad (8)$$

Where $y_c(t) = \cos(\omega_0 t + \alpha t^2/2 + \varphi_0)$ is the cosine component of the reference signal, $y_s(t) = \sin(\omega_0 t + \alpha t^2/2 + \varphi_0)$ is the sine component of the reference signal.

Direct calculation of the correlation function in accordance with the formula (8) did not produce a good correlation peak because of source motion during the 135-s sweep. This can be corrected by adjusting the sampling frequency of the reference signal.

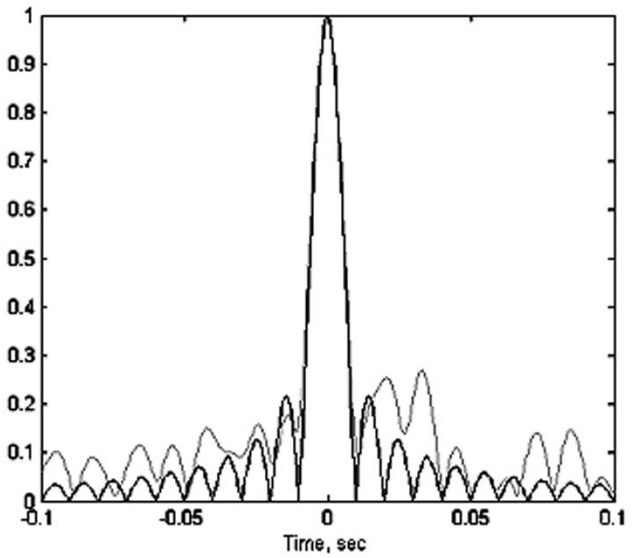

Fig. 18. Single-ray path correlation function of a swept frequency source: the black curve is a perfect theoretical correlation; the gray curve is the experimental correlation.

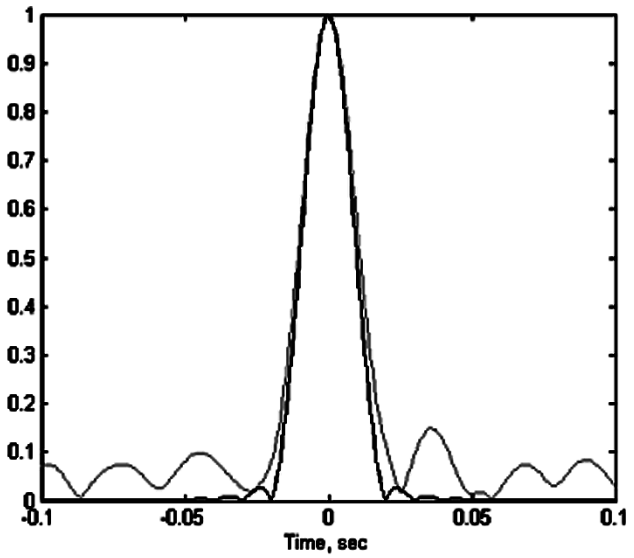

Fig. 19. Single-ray path correlation function of a swept frequency source, with Hann window: the black curve is a perfect theoretical correlation; the gray curve is the experimental correlation.

A linear model is used for the reference-signal time-scale correction. In accordance with that model, the reference signal time argument t is compared with the received signal time argument t' by the relationship of

$$t = t_0 + \alpha t' \tag{9}$$

where $\alpha = v/c$; v is the radial speed of the research vessel movement and c is the sound speed. The correction of the reference-signal time scale was realized with the help of a program, which searches on a digital set of coefficients α for the maximum correlation peak of a single received ray.

The corrected correlation function of a single-ray received signal after sampling frequency adjusting is presented in Fig. 18. The theoretical correlation function (autocorrelation function) of the reference signal is also shown in Fig. 18, by a black curve. Very good agreement of the theoretical and experimental curves in the area of the main peak should be emphasized. The correlation function sidelobes level is essentially decreased by applying correlation processing with the Hann window. The results of this process are presented in Fig. 19.

The amplitude of the correlation function is determined via the formula (10) [see (10) at the bottom of the page] where $W(t)$ is the Hann window-weight function and $\hat{\alpha}(t)$ is the estimation of the time scale. The autocorrelation function of the reference signal obtained by integration with the weight $W(t)$ is shown by the black color (perfect theoretical correlation function). Note that in spite of the considerable decrease in the potential level of sidelobes with the Hann weight function $W(t)$ applied, the sidelobes of the received signal correlation function remain at a level $\sim$ 0.1. This can easily be explained by weak energy scattering in the inhomogeneous water layer under the wavy sea surface.

VII. Conclusion

A computer simulation and numerous field tests of a low-frequency sound source with a variable resonant frequency has shown that this new approach to a projector design exhibits a high efficiency, high radiated power, and unlimited operational depth. A resonant tube sound source with a computer-controlled resonant frequency can be used for radiating broad-band swept frequency signals and narrow-band signals with the carrier in a large frequency range as well. Computer control enables holding the resonant frequency in compliance with the instantaneous signal frequency with a very small error. The correlation function of the linear frequency modulated signal is very close to the theoretical one. The frequency bandwidth of such a projector can reach a value 0.7 to 0.8 of the central frequency. A field test has shown that this sound-projector system is easily deployed and can operate on alkaline batteries for more then one year. This new sound-projector system is recommended as a simple low-cost sound source for deepwater research, such as ocean acoustic tomography in the frequency range of 50 to 1000 Hz.

$$c(t) = \sqrt{\left(\int_0^{T_c} y_s(t)(\hat{\alpha}t)x(t-\tau)W(t)dt\right)^2 + \left(\int_0^{T_c} y_s(\hat{\alpha}t)x(t-\tau)W(t)dt\right)^2} \tag{10}$$

ACKNOWLEDGMENT

The authors express sincere thanks to Dr. J. Lindberg from ONR for interesting and productive discussions and for support of this work. For the development of Tonpilz acoustical driver and for very helpful consultations during all research stages, the authors deeply thank T. Ensign, the president of Engineering Acoustics, Inc., Orlando, Florida. The authors also thank Dr. C.-S. Chiu from the Naval Postgraduate School (NPS), Monterey, CA; Dr. U. Send from the Institut fuer Meereskunde, Kiel, Germany; and Dr. T. Terre from the French Research Institution for Exploitation of the Sea (IFREMER), Brest, France, for sponsoring and participating in the projector sea trials.

REFERENCES

[1] W. Munk and C. Wunsch, "Ocean acoustic tomography: A scheme for large-scale monitoring," *Deep-Sea Res.*, vol. 26A, pp. 123–161, 1979.

[2] P. F. Worcester, R. C. Spindel, and B. W. Howe, "Reciprocal acoustic transmissions: Instrumentation for mesoscale monitoring of ocean currents," *IEEE J. Oceanic Eng.*, vol. OE-10, pp. 123–137, Apr. 1985.

[3] C. Gae, Y. L. Gall, and T. Terre, "For ocean acoustic tomography new modular instrumentation," *Sea Technol.*, vol. 55, pp. 55–58, 1999.

[4] G. R. Potty, J. H. Miller, J. F. Lynch, and K. B. Smith, "Tomographic inversion for sediment parameters in shallow water," *J. Acoust. Soc. Am.*, vol. 108, no. 3, pp. 973–986, 2000.

[5] R. S. Woollett, "Basic problems caused by depth and size constrains in low-frequency underwater transducers," *J. Acoust. Soc. Am.*, vol. 68, no. 4, pp. 1031–1037, 1980.

[6] G. W. McMahon, "Performance of open ferroelectric ceramic rings in underwater transducers," *J. Acoustic Soc. Am.*, vol. 36, pp. 528–533, 1964.

[7] J. B. Lee, "Low-frequency resonant-tube projector for underwater sound," in *Proc. IEEE Ocean'74*, vol. 2, N. S. Halifax, Ed., August 21–23, 1974, pp. 10–15.

[8] T. J. Rossby, J. Ellis, and D. C. Webb, "An efficient sound source for wide area RAFOS navigation," *J. Atmospheric & Oceanic Technol.*, vol. 10, no. 3, pp. 397–403, 1993.

[9] T. F. Duda, "Analysis of finite-duration wide-band frequency sweep signals for ocean tomography," *IEEE J. Oceanic Eng.*, vol. 18, pp. 87–94, Apr. 1993.

[10] B. L. Fanning and G. W. McMahon, "Vented-Pipe Projector," United States Patent 4 855 964, July 8, 1988.

[11] O. B. Wilson, "Introduction to the Theory and Design of Sonar Transducers," Peninsula, Los Altos, CA, 1988.

[12] A. Viterbi, *Principles of Coherent Communications (Systems Science)*. NY: McGraw-Hill, 1966.

Andrey K. Morozov was born in Moscow, Russia. He received the M.S. degree in radiophysics from the Moscow Power Engineering Institute (Technical University), Moscow, Russia, the M.S. degree in applied mathematics from the Moscow State University, Moscow, Russia, and the Ph.D. degree in 1981 from the Moscow Power Engineering Institute, Moscow, Russia.

In 1975, he was with the Moscow Power Engineering Institute as a Junior Research Scientist and then as a Senior Research Scientist and a Deputy Head of the radio-system department. From 1987 to 1998, he was with the P. P. Shirshov Institute of Oceanology Russian Academy of Sciences, Moscow, Russia, as a Senior Research Scientist and then as a Leading Research Scientist. From 1998 to 1999, he was a Visiting Professor at the Research Institute for Applied Mechanics, Kyushu University, Fukuoka, Japan. He joined Webb Research Corporation, Falmouth, MA, in 1999 as a Chief Scientist. Since 2001, he has been a Guest Investigator at the Woods Hole Oceanographic Institution, Woods Hole, MA. He has extensive research experience in the field of communications, signal processing, and underwater acoustics.

Douglas C. Webb was born in Ontario, Canada. He received the B.S. degree in electrical engineering from Queens University, Kingston, ON, Canada, in 1952 and the M.S. degree in electrical engineering from Manchester University, Manchester, U.K., in 1954.

He was with Ferranti Electric Company, Manchester, U.K., and Olivetti, Italy, before coming to the United States. In 1962, he was with the Woods Hole Oceanographic Institution, Woods Hole, MA. In 1982, he started Webb Research Corporation, Falmouth, MA, where he has continued the development of tools for the observation of the ocean interior. He is the author and coauthor of 41 publications.

Mr. Webb was awarded the Woods Hole Oceanographic Institution Bigelow Medal in 1988.